Dynamic structure factor and vibrational properties of SiO_2 glass

Wei Jin, Priya Vashishta, and Rajiv K. Kalia
Concurrent Computing Laboratory for Materials Simulations, Department of Physics and Astronomy and Department of Computer Sciences, Louisiana State University, Baton Rouge, Louisiana 70803-4001

José P. Rino
Universidade Federal de São Carlos, 13560 São Carlos, São Paulo, Brazil
(Received 13 May 1993)

Molecular-dynamics simulations are performed to determine dynamic correlations in SiO_2 glass. The frequency and eigenvectors of vibrational normal modes are obtained by diagonalizing the dynamical matrix. Dynamic structure factors, partial and total vibrational density of states (DOS), and participation ratios are calculated. The neutron-weighted dynamic structure factor, $S_n(q,\omega)$, exhibits all the important features observed in the inelastic-neutron-scattering experiments on SiO_2 glass. As a function of ω, $S_n(q,\omega)$ has two regions separated by a gap near 120 meV. The dominant features in $S_n(q,\omega)$ are the peaks around 10–20 meV, an almost monotonic decrease between 20 and 100 meV, the gap near 120 meV, and a broad peak between 130 and 160 meV. The dynamic structure factor oscillates with variations in q. The total phonon DOS show two well-delineated bands, a broad band between 5 and 110 meV and a narrow band between 120 and 180 meV. The modes below 100 meV are spatially extended, whereas the high-frequency modes are localized. Calculations of the generalized neutron-weighted effective density of states are compared with neutron-scattering experiments.

I. INTRODUCTION

Silica is a very important material in many respects.[1–4] It exists in both crystalline and glassy (amorphous) forms. Crystalline silica has a variety of polymorphs with widely varying densities.[4–7] In particular, cubic β-cristobalite is the lowest density (2.20 g/cm^3) and tetragonal stishovite is the highest density (4.29 g/cm^3) polymorph of silica. Except stishovite, whose structural units are distorted $Si(O_{1/3})_6$ octahedra, all stable phases of crystalline silica consist of $Si(O_{1/2})_4$ tetrahedral units.

For the past several decades, silica glass (a-SiO_2) has been the subject of much research effort because of its scientific, technological, and geophysical importance.[2,3] The structure of a-SiO_2 has been extensively studied by various experimental[7–14] and theoretical[15–17] methods, and by computer simulations.[18–26] X-ray (Refs. 8 and 9), neutron (Refs. 8, 10, and 14), and NMR (Ref. 11) experiments, and computer simulation (Refs. 18-20 and 23) studies indicate that a-SiO_2 consists of *corner-sharing* $Si(O_{1/2})_4$ tetrahedral units, similar to those in crystalline silica.

A variety of experimental techniques[27]— Raman and Brillouin scattering,[12,13] infrared reflectivity,[28] and inelastic neutron scattering[29–35] have been used to study atomic vibrations in SiO_2 glass. Inelastic neutron scattering (INS) is a particularly powerful probe of structural and dynamical correlations in disordered and amorphous solids,[36] since it gives an energy and wave-vector-dependent dynamic structure factor. The intensity of the coherent INS scattering from a vibrational mode depends on the relative positions of the atoms involved in such a mode and correlations between their displacement vector components.[32,37] Therefore, the measured dynamic structure factor can be used to infer information about the short- and intermediate-range order in glasses.

Leadbetter and Stringfellow[29] performed an INS experiment on a-SiO_2. They obtained the neutron-weighted effective phonon density of states using the "incoherent approximation." The experimental generalized neutron-weighted effective density of states (GDOS) revealed peaks at 45 and 98 meV and a broad peak from 115 to 160 meV. Galeener, Leadbetter, and Stringfellow[30] compared Raman and infrared spectra with the INS spectra of SiO_2 glass. They found the splitting of the peaks at 135 and 150 meV, which was observed earlier by Galeener and Lucovsky[28] from infrared measurements. Using INS experiments, Buchenau, Nücker, and Dianoux[33] have measured the low-energy (1–10 meV) portion of the effective phonon density of states. These results are interpreted in terms of coupled rotational motion of SiO_4 tetrahedra. Granéli and Dahlborg[34] have studied the temperature dependence of the neutron inelastic-scattering-structure factor of a-SiO_2. Using The Intense Pulsed Neutron Source at Argonne National Laboratory, Carpenter and Price performed extensive neutron-scattering measurements of SiO_2 glass.[31,32] From their measurements, the wave-vector and energy-dependent inelastic dynamic structure factors and the generalized vibrational density of states are obtained. Recently, Arai *et al.*[35] have performed high-resolution ($\Delta E/E \sim 1.5\%$) inelastic-neutron-scattering measurements of dynamic structure factors of a-SiO_2. Their generalized phonon density of states shows a shoulder at 10 meV, a broad peak around 50 meV, and sharp peaks at 100, 133, and 150 meV, in agreement with the measurements of Carpenter and Price.[31,32] Arai *et al.*[35] also observed a broad hump around 60 meV and weak peaks at 63 and 77 meV. Dynamic structure factors and general-

0163-1829/93/48(13)/9359(10)/$06.00

ized phonon densities of states of other oxide (GeO_2) and chalcogenide (Ge_xSe_{1-x}, Si_xSe_{1-x}) glasses have also been measured by inelastic neutron scattering.[38]

The vibrational properties of silica glass have been investigated by numerical simulations and analytical techniques.[39–49] Bell and Dean calculated the vibrational density of states and dynamic structure factor of a hand-built random-network model[16] of SiO_2 glass using a nearest-neighbor Born potential, which included central- and noncentral-force constants.[39,40] Bell and Hibbins-Butler[40,41] have calculated the infrared and Raman spectra of computer generated random-network model of SiO_2 glass. Laughlin and Joannopoulos[42] have used a Bethe-lattice model and Born potential to calculate neutron, infrared, and Raman spectra of SiO_2 glasses. Sen and Thorpe[43] (ST) have used "infinitely extended tetrahedral network" model with nearest-neighbor central forces to calculate vibrational frequencies of AX_2-type glasses ($AX_2=SiO_2$, $GeSe_2$, etc). In the case of SiO_2, Galeener[44] has found a reasonable fit to the peak positions in the neutron density of states and Raman spectra. Carpenter and Price[31] and Arai *et al.*[35] have used the ST model to fit the q variations of their neutron-scattering dynamic structure factors. Thorpe and Galeener[45] have extended the ST model to several other random-network structures. Guttman and Rahman[26] have used a different random-network model and the Keating[50] potential to calculate density of states for a-SiO_2. Mitra,[51] Garofalini,[52] and Alavi *et al.*[25] have calculated the power spectra of velocity-velocity autocorrelation functions of SiO_2 glass using molecular-dynamics (MD) simulations with effective two-body potentials.

In this paper we describe the results of molecular-dynamics simulations for dynamical correlations in a-SiO_2. The simulations are based on effective interatomic potentials,[23] which consist of two- and three-body interactions. The two-body potentials incorporate the effects of charge-transfer, steric repulsion, and electronic polarizability of atoms. The three-body potentials take into account the covalent interactions. This potential gives a fairly good description of structural properties of a-SiO_2. From these simulations, we have calculated the neutron-weighted dynamic structure factor, $S_n(q,\omega)$ as a function of ω and q, and the generalized neutron-weighted effective density of states $G_n(\omega)$. These functions are compared with inelastic neutron-scattering measurements. The calculated $S_n(q,\omega)$ exhibits all the important features observed in the inelastic neutron-scattering experiments on SiO_2 glass. As a function of ω, $S_n(q,\omega)$ has two regions separated by a gap near 120 meV. The dominant features in $S_n(q,\omega)$ are the peaks around 10–20 meV, an almost monotonic decrease between 20 and 100 meV, the gap near 120 meV, and the broad peak between 130 and 160 meV. The dynamic structure factor oscillates with variations in q.

The outline of this paper is as follows: In Sec. II we describe the interatomic potentials and the molecular-dynamics simulations for SiO_2 glasses. Structural characteristics of computer-generated SiO_2 glasses are also described in Sec. II. Results for the vibrational normal modes and the dynamic structural factors are described in Sec. III. The phonon density of states and the phase relationship between vibrating atoms are discussed in Sec. IV. Localization properties of the phonon modes are discussed in Sec. V. Section VI gives a conclusion.

II. MOLECULAR-DYNAMICS SIMULATIONS

The simulations reported here are based on an effective potential composed of two-body and three-body terms,

$$V(\{\mathbf{r}_i\})=\sum_{i<j}V_2(r_{ij})+\sum_{i<j<k}V_3(\mathbf{r}_{ij},\mathbf{r}_{jk},\mathbf{r}_{ik})\ , \tag{1}$$

where $\mathbf{r}_i$ is the position of the ith atom and $\mathbf{r}_{ij}=\mathbf{r}_j-\mathbf{r}_i$ is the vector distance between atoms i and j. The two-body potential is given by

$$V_2(r_{ij})=\frac{Q_iQ_j}{r_{ij}}-\frac{\frac{1}{2}(\alpha_iQ_j^2+\alpha_jQ_i^2)}{r_{ij}^4}\exp\left[-\frac{r_{ij}}{r_{4s}}\right]+\frac{H_{ij}}{r_{ij}^{\eta_{ij}}}\ , \tag{2}$$

where Q_i is the effective charge on and α_i is the electronic polarizability of the ith atom. In Eq. (2), the first term is the Coulomb interaction, the second term is the charge-dipole interaction, and the third term is the steric repulsion.

The three-body contributions include Si-O-Si and O-Si-O bond-stretching and bond-bending effects:

$$V_3(\mathbf{r}_{ij},\mathbf{r}_{jk},\mathbf{r}_{ik})=B_{jik}\exp\left[\frac{a}{r_{ij}-r_0}+\frac{a}{r_{ik}-r_0}\right][\cos\theta_{jik}-\cos\bar{\theta}_{jik}]^2\Theta(r_0-r_{ij})\Theta(r_0-r_{ik})\ , \tag{3}$$

where B_{jik} is the strength of the three-body potential, θ_{jik} is the angle between $\mathbf{r}_{ij}$ and $\mathbf{r}_{ik}$, and Θ is the step function. The parameters in Eqs. (2) and (3) were determined empirically from the crystal structures, cohesive energy, and melting temperature of the glass. The effective charges of Si and O are taken to be $+4Q$ and $-2Q$, respectively, where $Q=0.4|e|$ is the empirical effective charge transfer. Extensive descriptions of the potential parameters can be found in Ref. 23. The range of three-body interaction is taken to be 2.6 Å.

Molecular-dynamics simulations[53] were carried out for a system of 648 particles (216 Si and 432 O) in a cubic box of length $L=21.39$ Å. Periodic boundary conditions and minimum image convention were imposed. The long-range Coulomb contribution was calculated with the Ewald summation technique.[54] Equations of motion were

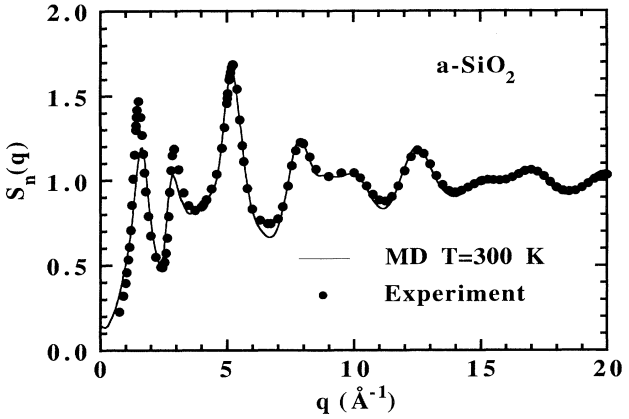

FIG. 1. Neutron static structure factors for a-SiO_2. Solid dots are the neutron-diffraction experimental results (Ref. 10). The solid line is the molecular-dynamics results at 300 K.

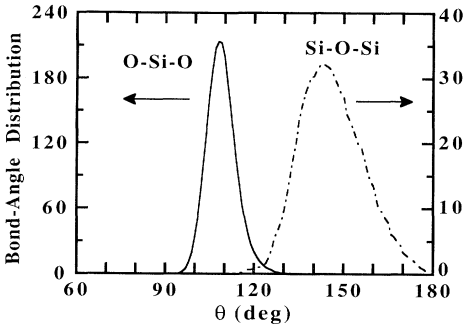

FIG. 2. Distribution of O-Si-O and Si-O-Si bond angles in a-SiO_2 at 300 K.

integrated with Beeman's algorithm[53] using a time step of $\Delta t = 0.5 \times 10^{-15}$ sec. The total energy of the system was conserved to at least 1 part in 10^4 over at least 10 000 MD time steps.

Starting from a well-equilibrated liquid state at ~3500 K and the experimental glass density ($\rho = 2.20 \text{g/cm}^3$), the system is cooled to another liquid state at 2500 K and thermalized for 60 000 time steps. This liquid state is further quenched by reducing the velocity of each particle by 0.01% at intervals of 10 time steps. Around 1500 K, where the system undergoes thermal arrest, it is thermalized for 60 000 time steps. Subsequently, the system is further quenched and thermalized to obtain glassy states at 600, 300, and 1 K. After equilibration at each temperature, structural, and dynamical properties are calculated with MD trajectories over 60 000 time steps (30 psec). The glass at 1 K was further quenched to zero temperature by the conjugate-gradient minimization method,[55] which corresponds to an infinite rapid quench.

Figure 1 shows a comparison between the calculated and experimental[16] neutron static structure factor, $S_n(q)$ for a-SiO_2. The prominent features in $S_n(q)$ are peaks at 1.60, 2.73, 5.11, 7.72, 12.33, and 16.75 Å^{-1} and shoulders around 9.76 and 15.05 Å^{-1}, where the first sharp diffraction peak (FSDP), the fingerprint of intermediate-range order, is at 1.6 Å^{-1}. Recently, Nakano, Kalia, and Vashishta have calculated $S_n(q)$ for a 41 472 particle system.[23] The height of the FSDP of this larger MD system is in excellent agreement with the neutron-diffraction experiments.

To further characterize the glass structure we have calculated the O-Si-O and Si-O-Si bond-angle distributions. The results are shown in Fig. 2. For an ideal tetrahedron, the O-Si-O angle is $\cos^{-1}(-1/3) = 109.47°$. The O-Si-O distribution in the glass is peaked at 109° with a full width at half maximum (FWHM) of 10°. Nearest-neighbor connectivity of tetrahedra is described by the Si-O-Si bond-angle distributions. In the glass, this distribution is asymmetric and peaked around 144° with a FWHM of 26°, indicating that there are no edge-sharing tetrahedra. The results of bond-angle distributions are in good agreement with NMR measurements.[11]

III. VIBRATIONAL NORMAL MODES AND DYNAMIC STRUCTURE FACTORS

The vibrational spectra can be calculated by diagonalizing the *dynamical matrix*. The *zero-force* configuration, $\{\mathbf{r}_i^0\}$ for the calculation of dynamical matrix is obtained by applying the conjugate-gradient method to a low-temperature glass configuration. The dynamical matrix is given by

$$D_{i\mu,j\nu} = (m_i m_j)^{-1/2} \left[\frac{\partial^2 V}{\partial r_{i\mu} \partial r_{j\nu}} \right]_0 ,$$
$$i,j = \{1,2,\cdots,N\}, \quad \mu,\nu = \{x,y,z\} , \tag{4}$$

where m_i is the mass of the ith atom. The dynamical matrix has $3N$ real eigenvalues (ω_n^2) with *real* eigenvectors. Many physical quantities of interest, such as the dynamic structure factor, infrared intensity, and density of states can be expressed in terms of the vibrational Green's function, $\mathbf{G}(\omega)$ given by

$$G_{\mu\nu}(i,j;\omega) = \sum_{n=1}^{3N} \frac{u_{i\mu}(n) u_{j\nu}^*(n)}{\omega^2 - \omega_n^2} , \tag{5}$$

where $u_{i\mu}(n) = m_i^{-1/2} A_{i\mu}(n)$ and $A_{i\mu}(n)$ is the $i\mu$ component of the *normalized* eigenvector.[56]

The coherent inelastic-neutron-scattering cross section is proportional to the neutron-weighted dynamic structure factor,[32,36,37] defined by the Fourier transform of the density-density correlation function, i.e.,

$$S_n(\mathbf{q},\omega) = \frac{1}{N\langle b^2 \rangle} \int_{-\infty}^{\infty} \frac{dt}{2\pi} e^{-i\omega t} \sum_{i=1}^{N} \sum_{j=1}^{N} b_i b_j \langle e^{i\mathbf{q}\cdot\mathbf{r}_j(t)} e^{-i\mathbf{q}\cdot\mathbf{r}_i(0)} \rangle , \tag{6}$$

where $\mathbf{q}$ is the scattering wave vector, b_i is the coherent neutron scattering length of atom i, $\langle b^2 \rangle = \sum_i b_i^2/N$, and $\mathbf{r}_j(t)$ is the position vector of atom j at time t. In Eq. (6), $\langle \cdots \rangle$ denotes the thermal average. Peaks in $S_n(\mathbf{q},\omega)$ correspond to collective excitations and their variations with $\mathbf{q}$ yield dispersion relations.

The neutron-weighted dynamic structure factor defined in Eq. (6) can be evaluated using MD trajectories. In the harmonic approximation, one can express the displacements in terms of the normal modes and expand[32] the exponents in the bracket into "phonon expansion," i.e., power serious in $\mathbf{q}\cdot\mathbf{u}$. The *one-phonon* contribution can be calculated from eigenvalues and eigenvectors of the dynamical matrix,[47]

$$S_n(\mathbf{q},\omega) = -\frac{q^2}{\pi N \langle b^2 \rangle} \mathrm{Im} \left[\sum_{i,j} \sum_{\mu,\nu} b_i b_j \hat{q}_\mu \hat{q}_\nu G_{\mu\nu}(i,j;\omega) e^{i\mathbf{q}\cdot(\mathbf{r}_i - \mathbf{r}_j)} \right] , \tag{7}$$

where the Debye-Waller factor and the Bose factor are omitted.[57]

Figure 3 displays the calculated one-phonon neutron-weighted dynamic structure factor for q between 0.3–16 Å^{-1} and for ω between 1–200 meV. The result at each q is an average over all $\mathbf{q}$ vectors of that amplitude. Periodic boundary conditions limit $\mathbf{q}$ to $(2\pi/L)(l_1,l_2,l_3)$, where l_i are integers. The lowest allowed value of q is restricted by the size of the system ($q_{\min} = 2\pi/L = 0.294$ Å^{-1}). Figure 3 indicates that for all values of q, there is a high-energy broad band between 130–160 meV, a less intense band near 100 meV, a rapid increase of the scattering function at lower energies, and little or no dispersion. The other dominant features in $S_n(q,\omega)$ are the peaks around 10–20 meV. These features are in reasonable agreement with the experimental INS measurements.[31,32] However, there are some discrepancies between the calculated and experimental results. In MD simulations, the broad band between 130–160 meV splits into three closely connected subbands with almost equal heights, whereas the experiment shows that this band splits into two bands. Figure 3 also indicates that phonons in the glass are almost dispersionless, a consequence of structural disorder. This is also found in neutron-scattering experiments.

Figure 4 displays the neutron-weighted dynamic structure factor as a function of q for several selected values of energy. The q^2 factor in $S_n(q,\omega)$ [Eq. (7)] has been taken out to reveal features that would otherwise be masked by this strong q dependence. Figure 4 reveals oscillation in $S_n(q,\omega)/q^2$ which is more pronounced at higher energies between 140–160 meV. Again, this is in agreement with neutron scattering experiments.[31,32,35]

To gain further insight into the neutron-weighted dynamic structure factor, we have examined the partial dynamic structure factor,

$$S_{\alpha\beta}(\mathbf{q},\omega) = \frac{1}{\sqrt{N_\alpha N_\beta}} \int_{-\infty}^{\infty} \frac{dt}{2\pi} e^{-i\omega t} \sum_{i\subset\alpha}^{N_\alpha} \sum_{j\subset\beta}^{N_\beta} \langle e^{i\mathbf{q}\cdot\mathbf{r}_j(t)} e^{-i\mathbf{q}\cdot\mathbf{r}_i(0)} \rangle , \tag{8}$$

where summations over i and j run over all atoms of type α and β, respectively. In terms of $S_{\alpha\beta}(\mathbf{q},\omega)$, the neutron-weighted dynamic structure factor can be written as

$$S_n(\mathbf{q},\omega) = \sum_\alpha \sum_\beta \frac{b_\alpha b_\beta}{\langle b^2 \rangle} (c_\alpha c_\beta)^{1/2} S_{\alpha\beta}(\mathbf{q},\omega) , \tag{9}$$

and the total density-density fluctuation spectra is given by

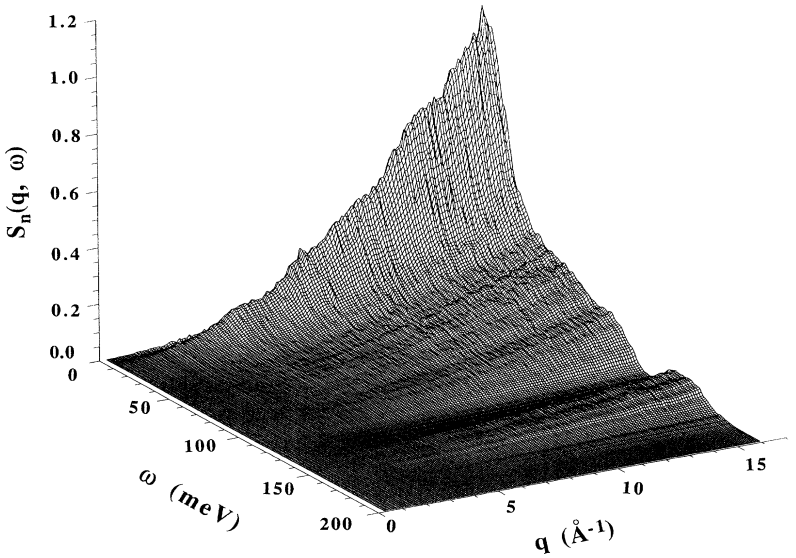

FIG. 3. Neutron-weighted dynamic structure factor $S_n(q,\omega)$ for a-SiO_2.

$$S(\mathbf{q},\omega)=\sum_{\alpha}\sum_{\beta}(c_\alpha c_\beta)^{1/2}S_{\alpha\beta}(\mathbf{q},\omega)\ . \tag{10}$$

The other interesting quantity is the charge-charge dynamic structure factor, defined by

$$S_{QQ}(\mathbf{q},\omega)=\frac{1}{N\langle Q^2\rangle}\int_{-\infty}^{\infty}\frac{dt}{2\pi}e^{-i\omega t}\langle\rho_Q(\mathbf{q},t)\rho_Q(-\mathbf{q},0)\rangle=\sum_{\alpha}\sum_{\beta}\frac{Q_\alpha Q_\beta}{\langle Q^2\rangle}(c_\alpha c_\beta)^{1/2}S_{\alpha\beta}(\mathbf{q},\omega)\ , \tag{11}$$

where Q_α is the effective charge on an atom of type α, $\langle Q^2\rangle=\sum_\alpha c_\alpha Q_\alpha^2$, and $\rho_Q(\mathbf{q},t)$ is the spatial Fourier components of the time-dependent microscopic charge-density,

$$\rho_Q(\mathbf{q},t)=\sum_{\alpha}\sum_{j\subset\alpha}^{N_\alpha}Q_\alpha e^{i\mathbf{q}\cdot\mathbf{r}_j(t)}\ . \tag{12}$$

Figure 5 displays Si-Si, Si-O and O-O partial dynamic structure factors and $S_{QQ}(q,\omega)$ for $q=2.59$, 5.59, and 15.60 Å^{-1}. Both $S_{\text{Si-Si}}(q,\omega)$ and $S_{\text{O-O}}(q,\omega)$ have maximum near $\omega\sim10$ meV, approach zero around 120 meV, and develop broad peak between 115 and 165 meV. In contrast, $S_{\text{Si-O}}(q,\omega)$ is small compared to $S_{\text{Si-Si}}(q,\omega)$ and $S_{\text{O-O}}(q,\omega)$ over the entire range of ω. Thus, the major contributions to the neutron dynamic structure factor arise from Si-Si and O-O partial dynamic correlations.

Figure 6 displays the wave vector dependence of $S_{\alpha\beta}(q,\omega)/q^2$ and $S_{QQ}(q,\omega)/q^2$ at 80 and 150 meV. All partial dynamic structure factors show q-oscillations. At

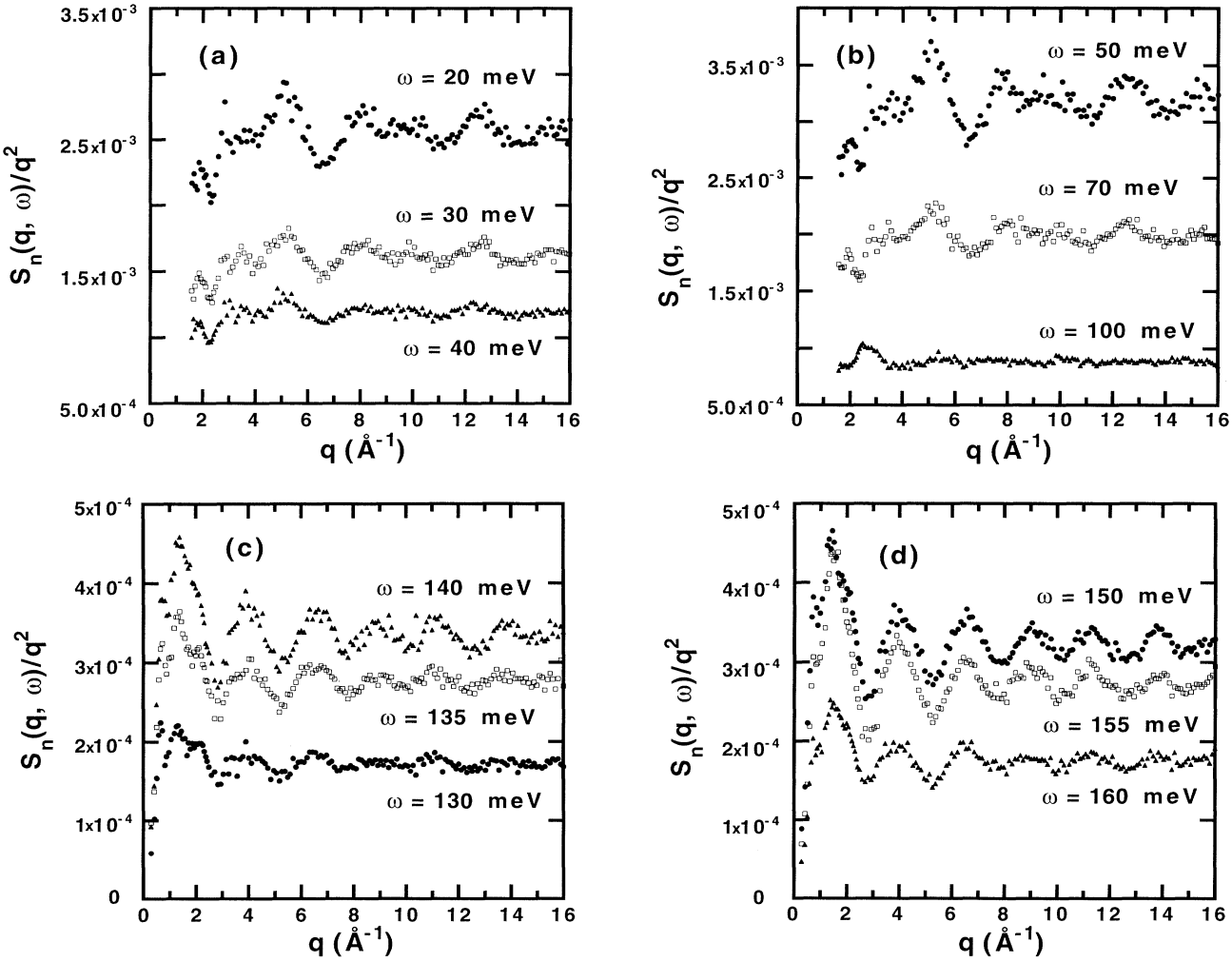

FIG. 4. Reduced neutron-weighted dynamic structure factor $S_n(q,\omega)/q^2$ for a-SiO_2 as a function of q at several selected values of ω. The results are calculated from Eq. (7), which involves a summation over delta-functions, $\sum_n\delta(\omega-\omega_n)$. In our calculations, the δ function has been broadened into a Gaussian of width 1.2 meV.

80 meV, amplitudes of these oscillations for Si-Si and Si-O are larger than the amplitude for the O-O oscillation. However, this behavior changes completely at 150 meV [Fig. 6(b)] where the dominant contribution to the neutron-weighted dynamic structure factor arise from O-O dynamic correlations.

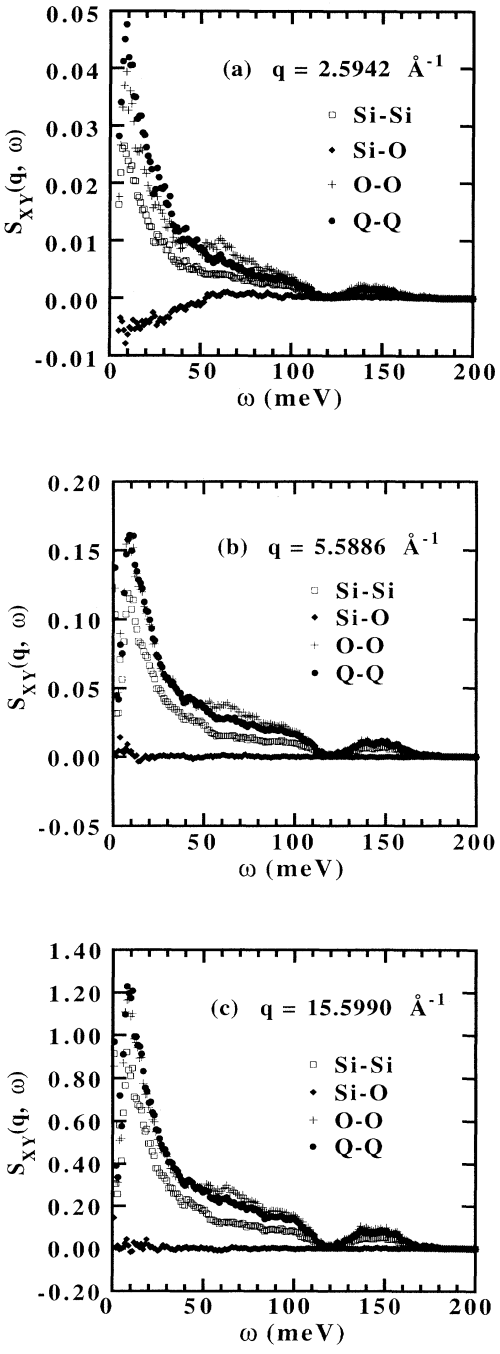

FIG. 5. Partial dynamic structure factors and charge-charge dynamic structure factor for a-SiO_2 as functions of energy at three selected values of q.

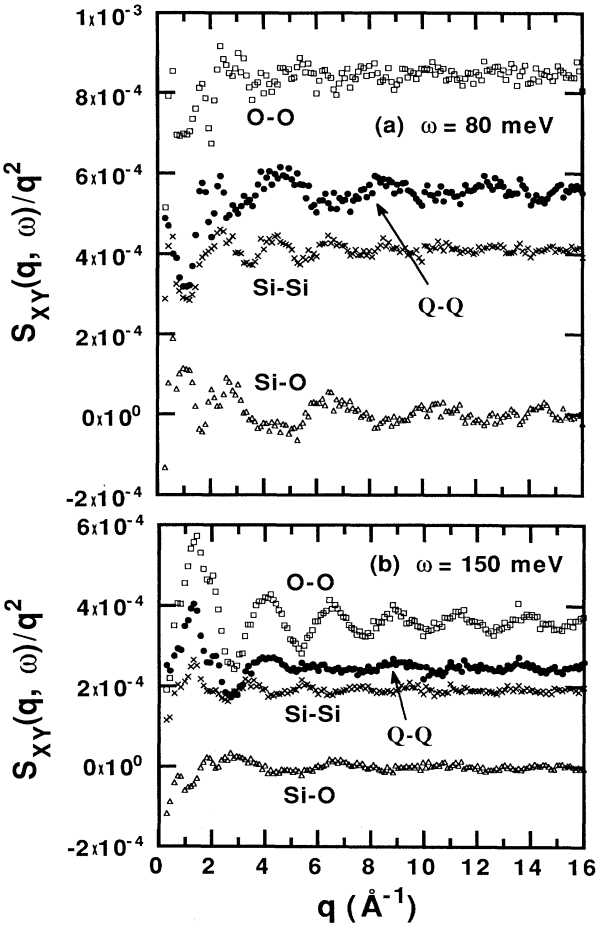

FIG. 6. Reduced partial dynamic structure factors and charge-charge dynamic structure factor for a-SiO_2 as functions of q at (a) 80 and (b) 150 meV.

IV. VIBRATIONAL DENSITY OF STATES

A. Density of states

The partial phonon density of states can be written in terms of the mass-weighted Green's function,[47]

$$F_\alpha(\omega) = -\frac{2\omega}{\pi} \sum_{i \subset \alpha}^{N_\alpha} \sum_{\mu} m_i \mathrm{Im}[G_{\mu\mu}(i,i;\omega)] \ . \tag{13}$$

Each term in the sum of Eq. (13) is referred to as *local* density of states (LDOS). The total DOS is given by $F(\omega) = \sum_\alpha F_\alpha(\omega)$. At low temperature, in the case of harmonic motion, the density of states can be calculated from the time Fourier transform of the velocity autocorrelation function.[58] Both these methods yield the same values of the DOS.

Figure 7 displays the partial and total vibrational DOS. Similar to the dynamic structure factor, the total DOS also displays a gap around 115 meV, separating the spectra into a broad lower band between 5 and 110meV and a higher band between 125 and 170 meV. The latter has three peaks at 139.5, 149.8, and 155.7 meV. The lower

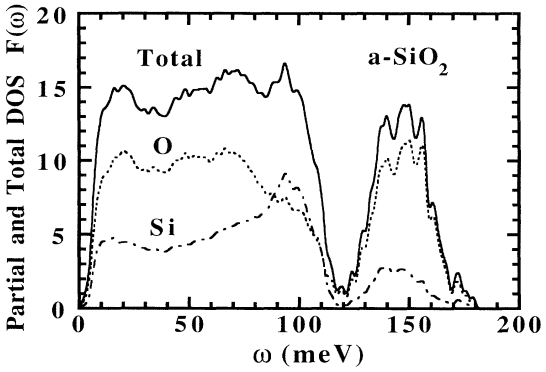

FIG. 7. Partial (Si and O) and total vibrational density of states for a-SiO_2.

band has broad peaks at 20, 48, and 66 meV. There is a narrow peak at 93.8 meV. In addition to these main peaks, there are weaker peaks around 34, 72, 99, 124, 129, and 172 meV.

Figure 7 also shows that both Si and O contribute significantly to the total DOS below 120 meV. The narrow peak near 93.8 meV is mainly due to Si, whereas the three peaks at 139.5, 149.8, and 155.7 meV are due to O.

Let us compare the calculated and experimental phonon spectra. Vibrational DOS of SiO_2 glass have been investigated by neutron,[29–35] infrared,[13,28,30] and Raman[13,30] scattering experiments. Inelastic neutron scattering measurements[29–31,35] of the GDOS reveal broad peaks centered around 50, 98, 133, and 150 meV.

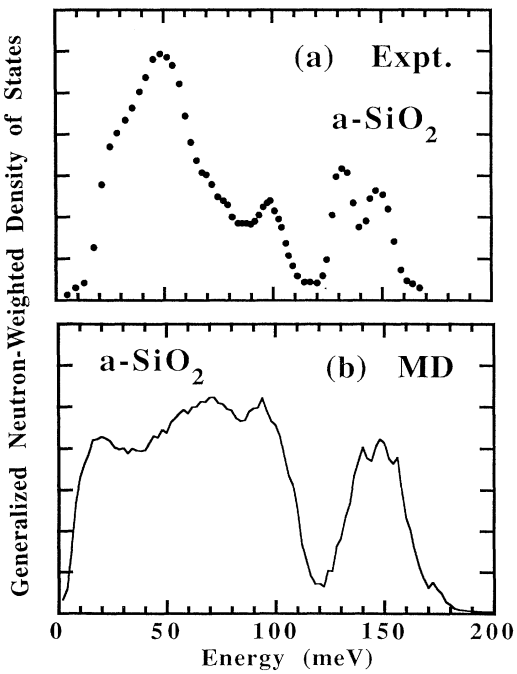

FIG. 8. Generalized neutron-weighted vibrational density of states $G_n(\omega)$ for a-SiO_2. Solid dots in (a) are inelastic neutron scattering experimental results (Refs. 31, 32).

Infrared spectra[28,30] reveal peaks at 50 and 130 meV, and the Raman spectrum[13] has strong features at 133 and 150 meV. The calculated DOS display most of the features observed experimentally, and the calculated peak positions differ less than 10% from the experimental results.

In a neutron-scattering experiment, it is often convenient to define a modified neutron-scattering function $G_n(\mathbf{q},\omega)$ by

$$G_n(\mathbf{q},\omega)\sim\omega S_n(\mathbf{q},\omega)/q^2 , \tag{14}$$

and introduce a generalized neutron-weighted effective density of states, $G_n(\omega)$, from the average of $G_n(q,\omega)$ over an extended range of q. Usually $G_n(\omega)$ is an *approximation* to the true vibrational density of states $F(\omega)$.[32]

Using $S_n(q,\omega)$, we calculate the GDOS and the results along with the experimental GDOS from INS experiments are shown in Fig. 8. The peak positions in the calculated GDOS are in reasonably good agreement with experimental results, although the shape of the experimental GDOS is quite different from the MD results.

B. Phase relations

Unlike crystals, phonons in glasses are not simply acoustic and optic. Vibrational modes in a glass can be classified as largely acoustic or optical depending on whether the atomic motions over the entire glass sample is in phase or out of phase. The eigenvectors contain all the information about the phase relationship between neighboring atoms. Bell and Hibbins-Butler[40,41] have proposed a scheme for assessing the phase relationship between neighboring atoms throughout the glass using the phase quotient

$$q_\Sigma(\omega_n)=\frac{\sum_{i,j}^{\text{bonds}} \mathbf{A}_i(n)\cdot\mathbf{A}_j(n)}{\sum_{i,j}^{\text{bonds}} |\mathbf{A}_i(n)\cdot\mathbf{A}_j(n)|} , \tag{15}$$

where $\mathbf{A}_i(n)$ is the normalized eigenvector of eigenmode n projected on atom i, and the summations are over nearest-neighbor atomic pairs (bonds). The function q_Σ is $+1$ for acoustic modes and -1 for optical modes. A similar phase quotient, $q_\sigma(\omega)$ for Si-O bond can be defined by Eq. (15) except the summation on ij is only over Si—O bonds.

Information about atomic motions parallel and perpendicular to Si—O bonds can also be obtained from

$$q_\parallel(\omega_n)=\frac{\sum_{i,j}^{ij=\text{Si—O}} \mathbf{A}_i(n)\cdot(\hat{\mathbf{r}}_{ij}\hat{\mathbf{r}}_{ij})\cdot\mathbf{A}_j(n)}{\sum_{i,j}^{ij=\text{Si—O}} |\mathbf{A}_i(n)\cdot(\hat{\mathbf{r}}_{ij}\hat{\mathbf{r}}_{ij})\cdot\mathbf{A}_j(n)|} \tag{16}$$

and

$$q_\perp(\omega_n)=\frac{\sum_{i,j}^{ij=\text{Si—O}} \mathbf{A}_i(n)\cdot(1-\hat{\mathbf{r}}_{ij}\hat{\mathbf{r}}_{ij})\cdot\mathbf{A}_j(n)}{\sum_{i,j}^{ij=\text{Si—O}} |\mathbf{A}_i(n)\cdot(1-\hat{\mathbf{r}}_{ij}\hat{\mathbf{r}}_{ij})\cdot\mathbf{A}_j(n)|} , \tag{17}$$

where $\hat{\mathbf{r}}_{ij}$ is the unit vector along the bond joining the equilibrium positions of atoms i and j. When all the neighboring Si and O atoms move along the Si—O bond, $q_{\parallel}$ is $+1$. On the other hand, $q_{\parallel}$ is -1 if all the neighboring Si and O atoms move in the direction opposite to each other along the Si—O bond.

Figure 9 displays the calculated phase quotients q_{Σ}, q_{σ}, $q_{\parallel}$, and $q_{\perp}$ in a-SiO_2. Evidently, q_{Σ} decreases from 0.9 to -0.5 as the energy increases from 5 to 90 meV. At higher energies, it first rises to -0.1 and then decreases to -0.75 around 160 meV. Clearly, the acoustic character of atomic vibration changes with the increases in the energy of phonon modes.

Figure 9 also shows that the phase factor q_{σ} drops smoothly from $+1$ to -1 around 110 meV. Below 30 meV, the Si-O motion is largely in phase. It gradually changes to out-of-phase motion between 50 and 110 meV. The phase factor $q_{\parallel}$ is $+1$ below 50 meV, drops to -1 at 110 meV, and then increases to -0.8 at 160 meV. The phase factor $q_{\perp}$ drops from $+1$ to -1 between 90 and 110 meV. Above 110 meV, $q_{\perp}$ increases again to ~ 0.5. At higher energies there are large fluctuations in the $q_{\perp}$ data, possibly due to small size of the simulation system.

V. LOCALIZATION OF PHONON MODES

Phonon localization can be inferred from a quantity called participation ratio,[59]

$$p_{\alpha}(\omega_n)=\left[\frac{1}{3N_{\alpha}}\right]\frac{\left\{\sum_{i\subset\alpha}^{N_{\alpha}}\sum_{\mu}[u_{i\mu}(n)]^2\right\}^2}{\sum_{i\subset\alpha}^{N_{\alpha}}\sum_{\mu}[u_{i\mu}(n)]^4} \quad (\alpha=\mathrm{Si,O}) . \tag{18}$$

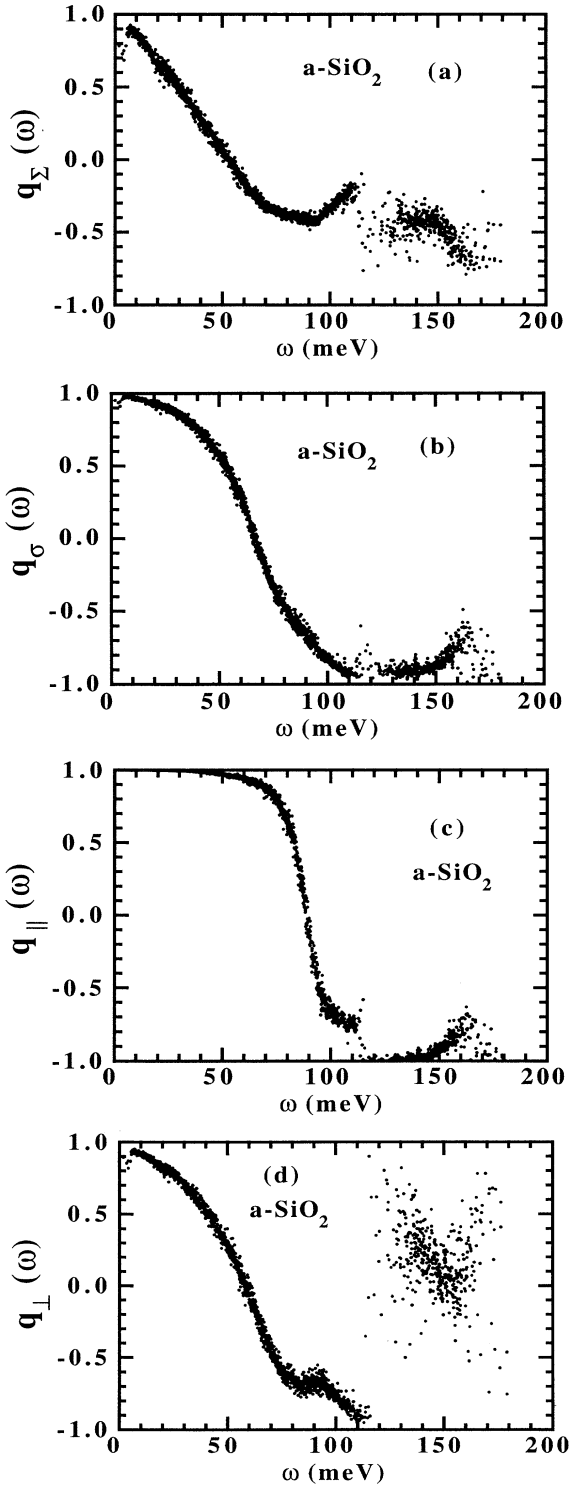

FIG. 9. Phase quotients $q_{\Sigma}(\omega)$, $q_{\sigma}(\omega)$, $q_{\parallel}(\omega)$, and $q_{\perp}(\omega)$ for a-SiO_2.

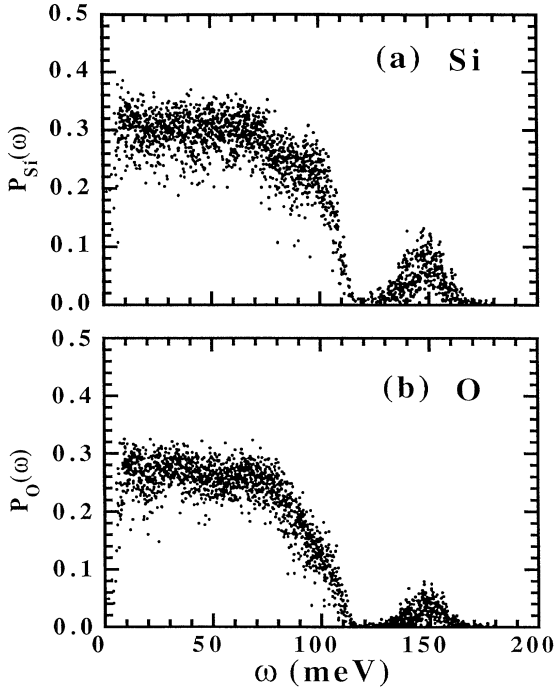

FIG. 10. (a) Si and (b) O partial participation ratios for a-SiO_2.

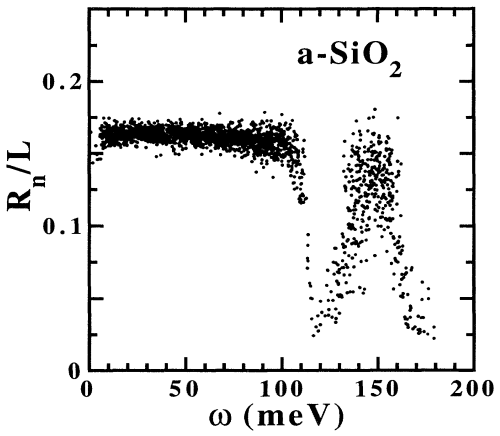

FIG. 11. Radius of gyration, R_n/L for a-SiO_2.

For extended modes, p_α is of order unity, whereas for localized modes, it scales inversely with N_α.

Figure 10 shows the partial participation ratios for Si and O. In both cases, the participation ratios are ~ 0.35 at low energies. They decrease sharply to zero near 115 meV. The low-energy modes ($5 < \omega < 100$meV) are extended and the high-energy modes are localized.

Following Yonezawa,[60] we define an effective "radius of gyration," R_n, of an eigenmode n by

$$R_n^2 = \frac{1}{3} \sum_\mu [\langle X_\mu(n)^2 \rangle - \langle X_\mu(n) \rangle^2] , \tag{19a}$$

$$\langle X_\mu(n)^2 \rangle = \sum_{i=1}^{N} |A_{i\mu}(n)|^2 (r_{i\mu} - r_{M\mu})^2 , \tag{19b}$$

and

$$\langle X_\mu(n) \rangle = \sum_{i=1}^{N} |A_{i\mu}(n)|^2 (r_{i\mu} - r_{M\mu}) , \tag{19c}$$

where M is the index of the atom that has the *largest amplitude* of eigenvector in the nth normal mode. If a mode is localized on a single atom, $R_n = 0$. For an extended mode, R_n is the average root-mean-square distance.

Figure 11 displays the results for R_N/L. Below 100 meV, $R_n/L \sim 0.16$ and around 110 meV, it declines rapidly to a value of 0.05. However, it increase again to 0.15 around 150 meV and drops to 0.01 near 170 meV.

VI. CONCLUSIONS

We have reported MD results for dynamic correlations in SiO_2 glass. The neutron-weighted dynamic structure factor, $S_n(q,\omega)$, partial and total vibrational density of states, and participation ratio are calculated. The dynamic structure factor shows the same features as observed in inelastic-neutron-scattering experiments. The calculated total phonon DOS has two well-delineated bands, a broad lower band between 5 and 110 meV and a narrow higher band between 120 and 180 meV. The higher band has three narrow peaks at 139.5, 149.8, and 155.7 meV. The lower-energy broad has peaks at 20.0, 48.0, and 66.0 meV, and a narrow peak at 93.8 meV. The low-frequency modes are spatially extended, whereas the high-frequency modes are spatially localized. We have also investigated the phase relationship between neighboring atoms to distinguish between the acoustic and optical character of phonon modes. The calculated dynamic structure factor and peak positions in the density of states are in satisfactory agreement with experimental results. However, the calculated GDOS is quite different in shape from the one obtained by INS experiments.

ACKNOWLEDGMENTS

We thank Dr. S. W. de Leeuw, Dr. A. Nakano, and Dr. J. Yu for useful discussions. This work was supported by the U. S. Department of Energy, Office of Energy Research, Basic Energy Science, Materials Science Division, Grant No. DE-FG05-92ER45477. The computations were performed using the computing facilities in the Concurrent Computing Laboratory for Materials Simulations (CCLMS) at Louisiana State University. The facilities in the CCLMS were acquired with the Equipment Enhancement Grants awarded by the Louisiana Board of Regents through Louisiana Education Quality Support Fund (LEQSF).

[1] R. Zallen, *The Physics of Amorphous Solids* (Wiley, New York, 1983).

[2] J. Zarzycki, *Glasses and the Vitreous States* (Cambridge University Press, New York, 1991); in *Basic Features of The Glassy State,* edited by J. Colmenero and A. Alegria (World Scientific, Singapore, 1990), p. 3.

[3] *The Physics and Technology of Amorphous SiO_2*, edited by R. A. B. Devine (Plenum, New York, 1988).

[4] I. Fanderlik, *Silica Glass and Its Applications* (Elsevier, Amsterdam, 1991).

[5] R. W. G. Wyckoff, *Crystal Structures* (Wiley, New York, 1965), Vol. 1, pp. 313–322.

[6] F. Liebau, in *The Physics and Technology of Amorphous SiO_2*, Ref. 3, p. 15.

[7] J. J. Pluth, J. V. Smith, and J. Faber, Jr., J. Appl. Phys. **57**, 1045 (1985); L. Levine, C. T. Prewitt, and D. J. Weidner, Am. Mineral. **65**, 920 (1980); L. Liu, W. A. Bassett, and T. Takahashi, J. Geophys. Res. **79**, 1160 (1974).

[8] S. C. Moss and D. L. Price, in *Physics of Disordered Materials,* edited by D. Adler, H. Fritzsche, and S. R. Ovshinsky (Plenum, New York, 1985), p. 77.

[9] R. L. Mozzi and B. E. Warren, J. Appl. Crystallogr. **2**, 164 (1969).

[10] R. N. Sinclair and A. C. Wright, J. Non-Cryst. Solids **57**, 447 (1983); P. A. V. Johnson, A. C. Wright, and R. N. Sinclair, *ibid.* **58**, 109 (1983).

[11] R. Dupree and R. F. Pettifer, Nature (London) **308**, 523 (1984); R. F. Pettifer *et al.*, J. Non-Cryst. Solids **106**, 408 (1988).

[12] M. Grimsditch, Phys. Rev. Lett. **52**, 2379 (1984); Phys. Rev. B

34, 4372 (1986); A. Polian and M. Grimsditch, *ibid.* **41**, 6086 (1990).

[13]R. J. Hemley *et al.*, Phys. Rev. Lett: **57**, 747 (1986); Q. Williams and R. Jeanloz, Science **239**, 902 (1988).

[14]S. Susman *et al.*, Phys. Rev. B **43**, 11 076 (1991).

[15]W. H. Zachariasen, J. Am. Chem. Soc. **54**, 3841 (1932); S. R. Elliot, Nature (London) **354**, 445 (1991).

[16]R. J. Bell and P. Dean, Nature (London) **212**, 1354 (1966); Philos. Mag. **25**, 1381 (1972).

[17]P. H. Gaskell and I. D. Tarrant, Philos. Mag. B **42**, 265 (1980).

[18]L. V. Woodcock, C. A. Angell, and P. Cheeseman, J. Chem Phys. **65**, 1565 (1976).

[19]S. K. Mitra *et al.*, Philos. Mag B **43**, 265 (1981); J. D. Kubicki and A. C. Lasaga, Am. Mineral. **73**, 941 (1988); T. F. Soules, J. Chem Phys. **71**, 4570 (1979); J. Non-Cryst. Solids **49**, 29 (1982); **73**, 315 (1985); L. Stixrude and M. S. T. Bukowinski, Phys. Rev. B **44**, 2523 (1991).

[20]B. Feuston and S. H. Garofalini, J. Chem Phys. **89**, 5818 (1988); **91**, 564 (1989).

[21]J. R. Rustad, D. A. Yuen, and F. J. Spera, Phys. Rev. B **44**, 2108 (1991).

[22]J. S. Tse, D. D. Klug, and Y. Le Page, Phys. Rev. B **46**, 5933 (1992); Phys. Rev. Lett. **69**, 3647 (1992); N. Binggeli and J. R. Chelikowsky, *ibid.* **69**, 2220 (1992); Nature (London) **353**, 344 (1991).

[23]P. Vashishta, R. K. Kalia, J. P. Rino, and I. Ebbsjö, Phys. Rev. B **41**, 12 197 (1990); A. Nakano, R. K. Kalia, and P. Vashishta (unpublished).

[24]W. Jin *et al.*, in *Strongly Coupled Plasma Physics,* edited by H. M. Van Horn and S. Ichirmaru (North-Holland, Amsterdam, in press); J. P. Rino *et al.*, Phys. Rev. B **47**, 3053 (1993).

[25]A. Alavi, L. J. Alvarez, S. R. Elliott, and I. R. McDonald, Philos. Mag. B **65**, 489 (1992).

[26]L. Guttman and S. M. Rahman, Phys. Rev. B **33**, 1506 (1986); J. Non-Cryst. Solids **75**, 419 (1985).

[27]R. M. Almeida, J. Non-Cryst. Solids **106**, 347 (1988).

[28]F. L. Galeener and G. Lucovsky, Phys. Rev. Lett. **37**, 1477 (1976).

[29]A. J. Leadbetter and M. W. Stringfellow, in *Neutron Inelastic Scattering* (International Atomic Energy Agency, Vienna, 1974), p. 501.

[30]F. L. Galeener, A. J. Leadbetter, and M. W. Stringfellow, Phys. Rev. B **27**, 1052 (1983).

[31]J. M. Carpenter and D. L. Price, Phys. Rev. Lett. **54**, 441 (1985). In this experiment, the SiO_2 glass sample was kept at 20 K to reduce multiphonon scattering, the neutron-scattering measurements were made with a pulsed neutron beam, and the measured scattering function $S(q,E)$ was interpolated into *a* q-E grid and corrected for multiple scattering effects.

[32]D. L. Price and J. M. Carpenter, J. Non-Cryst. Solids **92**, 153 (1987).

[33]U. Buchenau, N. Nücker, and A. J. Dianoux, Phys. Rev. Lett. **53**, 2316 (1984); U. Buchenau *et al.*, Phys. Rev. B **34**, 5665 (1986).

[34]B. Granéli and U. Dahlborg, J. Non-Cryst. Solids **109**, 295 (1989).

[35]M. Arai, A. C. Hannon, A. D. Taylor, A. C. Wright, R. N. Sinclair, and D. L. Price (unpublished).

[36]K. Suzuki, in *Neutron Scattering,* edited by D. L. Price and K. Skold (Academic, New York, 1987), Pt. B, p. 243; K. Crawford, Neutron News **1** (9), 9 (1990).

[37]J. M. Carpenter and C. A. Pelizzari, Phys. Rev. B **12**, 2397 (1975); **12**, 2397 (1975).

[38]U. Walter *et al.*, Phys. Rev. B **37**, 4232 (1988); M. Arai *et al.*, *ibid.* **37**, 4240 (1988); L. F. Gladden *et al.*, J. Non-Cryst. Solids **106**, 120 (1988).

[39]P. Dean, Rev. Mod. Phys. **44**, 127 (1972); R. J. Bell, Rep. Prog. Phys. **35**, 1215 (1972).

[40]R. J. Bell, in *Methods in Computational Physics* (Academic, New York, 1976), Vol. 15, p. 215; in *Excitations in Disordered Systems,* edited by M. F. Thorpe (Plenum, New York, 1981), pp. 333 and 347.

[41]R. J. Bell and D. C. Hibbins-Butler, J. Phys. C **3**, 2111 (1970); **4**, 1214 (1971); **8**, 787 (1975); **9**, 1171 (1976).

[42]R. B. Laughlin and J. D. Joannopoulos, Phys. Rev. B **16**, 2942 (1977).

[43]P. N. Sen and M. F. Thorpe, Phys. Rev. B **15**, 4030 (1977).

[44]F. L. Galeener, Phys. Rev. B **19**, 4249 (1979); in *The Physics and Technology of Amorphous* SiO_2, Ref. 3, p. 1; in *Disorder in Condensed Matter Physics,* edited by J. A. Blackman and J. Tagüeña (Oxford University Press, Oxford, 1991), p. 45.

[45]M. F. Thorpe and F. L. Galeener, Phys. Rev. B **22**, 3078 (1980); F. L. Galeener and M. F. Thorpe, *ibid.* **28**, 5802 (1983).

[46]J. R. Banavar and J. C. Phillips, Phys. Rev. B **28**, 4716 (1983).

[47]S. W. de Leeuw and M. F. Thorpe, Phys. Rev. Lett **55**, 2879 (1985); J. Non-Cryst. Solids **75**, 393 (1985); M. F. Thorpe and S. W. de Leeuw, Phys. Rev. B **33**, 8490 (1986).

[48]R. A. Murray and W. Y. Ching, Phys. Rev. B **39**, 1320 (1989).

[49]A. Lehmann, L. Schumann, and K. Hübner, Phys. Status Solid. B **117**, 689 (1983).

[50]P. N. Keating, Phys. Rev. **145**, 637 (1966).

[51]S. K. Mitra, Philos. Mag. B **45**, 529 (1982).

[52]S. H. Garofalini, J. Chem. Phys. **76**, 3189 (1982); J. Non-Cryst. Solids **120**, 1 (1990).

[53]A. Rahman and P. Vashishta, in *The Physics of Superionic Conductors and Electrode Materials,* edited by J. W. Perram (Plenum, New York, 1983), p. 93.

[54]J. P. Hansen, in *Molecular-Dynamics Simulation of Statistical-Mechanical Systems,* edited by G. Ciccotti and G. W. Hoover (North-Holland, Amsterdam, 1986), p. 89.

[55]R. Fletcher, *Practical Methods of Optimization* (Wiley, New York, 1980).

[56]The eigenvector $\mathbf{A}(n)$ of the nth normal mode forms a complete orthonormal set with 3N components. The eigenvectors are normalized to unity such that $\sum_{i\mu} A_{i\mu}(n) A_{i\mu}(m) = \delta_{nm}$.

[57]Note that the notation $\mathbf{r}_i$ from now on is equivalent to the notation $\mathbf{r}_i^0$ used previously.

[58]A. Rahman, M. J. Mandell, and J. P. McTague, J. Chem. Phys. **64**, 1564 (1976).

[59]S. R. Nagel, G. S. Grest, and A. Rahman, Phys. Rev. Lett. **53**, 368 (1984); R. Biswas *et al.*, *ibid.* **60**, 2280 (1988).

[60]F. Yonezawa, J. Non-Cryst. Solids **35/36**, 29 (1980).